Journal of Luminescence 229 (2021) 117702

Contents lists available at ScienceDirect

Journal of Luminescence

journal homepage: http://www.elsevier.com/locate/jlumin

Full Length Article

Phase transition of YPO_4 crystal induced splitting of $^5D_0 \rightarrow {}^7F_1$ of doped Eu^{3+} ions

Faizan Raza [1], Tian Dong [1], Peng Li, Habib Ullah, Huanrong Fan, Yanpeng Zhang [*]

Key Laboratory for Physical Electronics and Devices of the Ministry of Education & Shaanxi Key Lab of Information Photonic Technique, Xi'an Jiaotong University, Xi'an, 710049, China

A B S T R A C T

For the first time, we investigated the crystal field dependent fine structure splitting in different crystal phases (pure tetragonal (T), pure hexahedral (H), (H + T) and (T + H)) of Eu^{3+}:YPO_4 crystals. We observed that each phase with its unique point group site symmetry results in unique fine structure splitting. The fine structure of T-phase and H-phase splits into two- and three-energy levels, respectively. By controlling temperature, the influence of dressing-phonon competition on the linewidth of spectral signal is also discussed. In T-phase Eu^{3+}:YPO_4, one spectral peak splits into three peaks under the action of stress and dressing field as temperature is reduced from 300 K to 77 K. The relationship between temporal and spectral intensity in different phases of Eu^{3+}:YPO_4 is also discussed. The Pr^{3+} ion has a stronger dressing than the Eu^{3+} ion in a host material of YPO_4 which can be explained from higher dipole moment. To further explore this comparison, we investigated intensity-noise correlation under nonlinear phase controlled by time delay in both Eu^{3+}:YPO_4 and Pr^{3+}:YPO_4.

Authorship contribution statement

Faizan Raza: Formal analysis, Data curation, Writing - original draft. Tian Dong: Formal analysis, Data curation, Writing - original draft. Peng Li: Funding acquisition, Data curation. Habib Ullah: Funding acquisition, Data curation. Huanrong Fan: Funding acquisition, Data curation. Yanpeng Zhang: Conceptualization, Methodology.

1. Introduction

Since trivalent Eu^{3+} and Pr^{3+} ions are extremely sensitive to the site symmetry and the surrounding crystal-field (CF) of the host material than other crystal ions, which makes them an attractive material for important applications such as in scintillation detectors, medical imaging and display devices. The crystal structure of YPO_4 mainly exists in two polymorphic forms, hexagonal (H-) and tetragonal (T-) phases [1,2]. The hexagonal-phase and tetragonal-phase occupy a D_2 and D_{2d} point-group symmetry site, respectively [3,4]. The luminescence intensity of H-phase Eu^{3+} YPO_4 crystal is higher than the T-phase Eu^{3+}-YPO_4 crystal [5,6]. The spectral properties of T-phaseYPO_4 crystal has been widely studied. It has been observed that the spectral behavior depends on the site symmetry of the crystal, exciting light, and temperature around phase [7].

Based on the Judd-Ofelt (JO) theory and the selection rules for electric-dipole (ED) and magnetic-dipole (MD) transitions [8,9], the intensity ratio of the $^5D_0$ - $^7F_2$ transition to the $^5D_0$ - $^7F_1$ transition of can thereby provide site symmetry information according to the JO [10,11]. Moreover, according to the ED selection rule, the $^5D_0$ - $^7F_0$ transition of induced by crystal field, J-mixing is present in the emission spectrum, which is only allowed for the following 10 site symmetries C_s, C_1, C_n and C_{nv} (n = 2, 3, 4,6) [12,13]. The polarization dependences of four-wave mixing (FWM) and the enhanced FWM have been studied [14]. The fluorescence (FL) spectra under the different polarizations of probe and pump fields have been reported theoretically and experimentally using such crystal [15–17]. The electromagnetically induced transparency (EIT) process can be controlled by selecting different transitions among Zeeman sublevels via the polarization states of the laser beams shining on atomic crystals [18]. In the atomic system, the polarization of the incident laser beams plays an important role in atomic transitions of multi-Zeeman energy-levels. The atomic Autler–Townes (AT) splitting was first observed on a radio frequency transition [19] and then in calcium atoms [20].

In contrast to previous research that focused on spectral behavior of YPO_4 [4], we report the fine structure splitting under crystal field in Eu^{3+} doped with YPO_4 nano-/microcrystals. Splitting of fine spectra can be effected by the phase transition of $^5D_0$ - $^7F_1$ in YPO_4 crystals. The proportion of phase in each crystal as follows: pure T-phase YPO_4, pure H-phase YPO_4, (40% T-phase with 60% H-phase) YPO_4 and (40%

* Corresponding author.
E-mail address: ypzhang@mail.xjtu.edu.cn (Y. Zhang).
[1] Faizan Raza and Tian Dong contributed equally to this work.

https://doi.org/10.1016/j.jlumin.2020.117702
Received 5 May 2020; Received in revised form 20 September 2020; Accepted 13 October 2020
Available online 19 October 2020

H-phase with 60% T-phase) YPO_4. The significant effect of crystal fields on fine spectra splitting can be observed from pure T-phase Eu^{3+}:YPO_4 at low temperature (77 K) under the action of dressing and stress. Further, we reinforce the dressing sensitivity of Pr^{3+} ion over Eu^{3+} using intensity-noise correlation. Furthermore, we explored the dependence of dressing on different doped ion (Eu^{3+} and Pr^{3+}) in host crystal of YPO_4. We discussed that the amplitude of two-mode intensity-noise correlation can be switched from negative to positive by manipulating non-linear phase through gate position.

2. Experimental setup

The sample has 5% concentration of doped Eu^{3+}/Pr^{3+} ions in host YPO_4 crystal. Synthesis of each Eu^{3+} (5%-doped YPO_4 samples with different structures: By dissolving Y_2O_3 and Eu_2O_3 in HNO_3 solution with agitation under heating, the $Y_{0.95}Eu_{0.05}$ $(NO_3)_3$ aqueous solution (0.4 M) was obtained. Then, 10 mL of $NH_4H_2PO_4$ solution (0.2 M) was added dropwise into the 5 mL of $Y_{0.95}Eu_{0.05}$ $(NO_3)_3$ solution (0.4 M) under continuous stirring for about 30 min. The pH value of the mixture was adjusted to about 1 by using the addition of HNO_3 solution. After vigorous stirring for 1 h, the resulting suspension was poured into the Teflon lined stainless steel autoclaves and then heated at 180 °C for 9 h. As the autoclave cooled to room temperature naturally, we washed the white precipitates with distilled water and absolute ethanol by centrifugation, followed by drying them for 12 h at 80 °C to collect the final Eu^{3+} -doped YPO_4 samples within pure H-phase YPO_4. Taking the same way but adjusting the concentration of the $NH_4H_2PO_4$ solution dropped into the $Y_{0.95}Eu_{0.05}$ $(NO_3)_3$ solution (0.4 M), the samples having different phases from hexagonal to tetragonal can be obtained.

Fig. 1(a) shows the crystal field splitting of fine structure ($^5D_0 \rightarrow {}^7F_1$) of Eu^{3+}:YPO_4 crystal. The $^7F_1$ fine structure (J = 1) splits into three levels (2J+1) under the crystal field effect of YPO_4. Fig. 1(b) shows the schematic diagram of the experimental setup. To implement this experiment, the sample was held in a cryostat (CFM-102 32S) whose temperature was controlled by flowing liquid nitrogen. The tunable dye laser which has 0.04 cm^{-1} linewidth is pumped by an injection-locked single-mode Nd: YAG laser (DLS 9010) with 10 Hz repetition rate and 5 ns pulse width is used to generate the pumping field $\boldsymbol{E}$ (ω, Δ) with detuning $\Delta = \Omega_{mn}-\omega$, here Ω_{mn} represents the frequency of atomic transition between levels and ω is the laser frequency. The generated second-order FL signal is detected by a photomultiplier tube (PMT), which is attached with a boxcar gated integrator and oscilloscope. The arrangement of PMT with respect to the sample is shown in Fig. 1(b). In our experiment, typical Rabi frequency and radiation intensity is about 1 GHz and 7.96 × 108 W/cm^2, respectively. The spectral signals are obtained by scanning laser frequency, while time-domain signals are obtained by fixing laser frequency.

3. Theoretical MODEL

In the two-level system, FL is generated by opening field E. The second-order FL can be expressed via the Liouville pathway $\rho_{00}^{(0)} \xrightarrow{E} \rho_{10}^{(1)} \xrightarrow{E'} \rho_{11}^{(2)}$. Thus, from perturbation chain, one can obtain the corresponding density matrix element using [21].

$$\rho_{11}^{(2)} = \frac{-|G|^2}{\left(\Gamma_{10} + i\Delta + |G|^2 / \Gamma_{00}\right)\left(\Gamma_{11} + |G|^2 / \left(\Gamma_{10} + i\Delta\right)\right)} \tag{1}$$

Where $G_i = \mu_i E_i/\hbar$ is the Rabi frequency of the field $\boldsymbol{E}$ with the electric dipole matrix elements μij of levels $|i\rangle$ and $|j\rangle$ and $\Gamma_{FL} = \Gamma_{10} + \Gamma_{11}$ is transverse decay rate of FL. The linewidth of the measured fluorescence signal is determined by the longitudinal relaxation time (T_1) and transverse relaxation time (T_2), that is, $\Gamma = (2\pi T1)^{-1} + (2\pi T2)^{-1}$, where T_1 is determined by the width of energy level and T_2 by the dephasing rate. Considering the interaction between the rare-earth doped crystal and coupling fields, the broadened linewidth of the measured FL signal can be described as

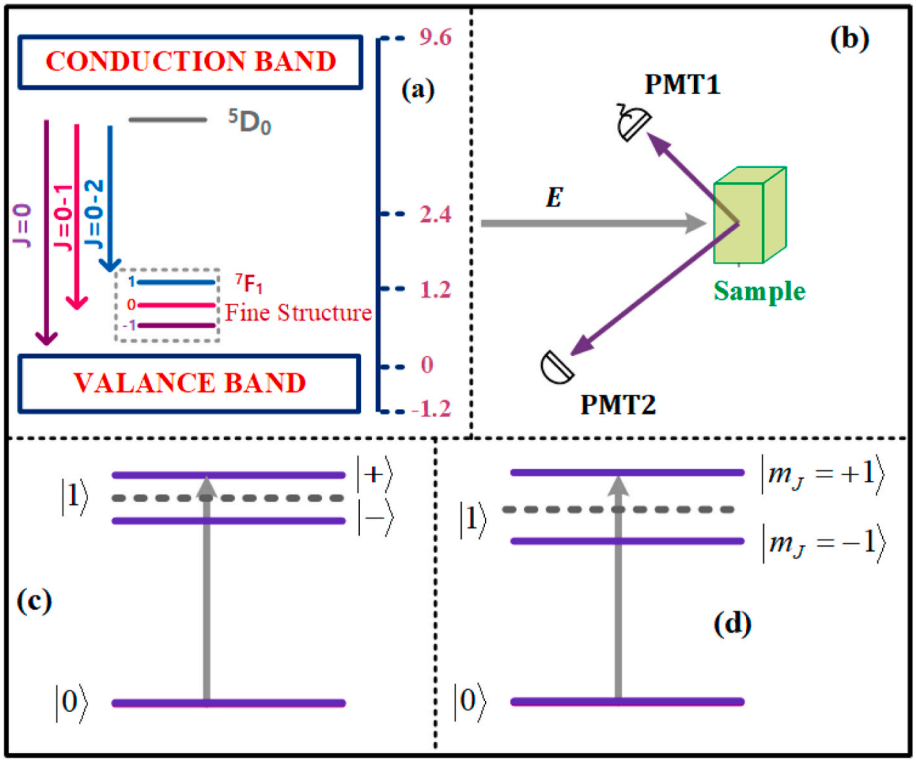

Fig. 1. (a) Fine structure energy levels of Eu^{3+}:YPO_4 crystal. (b) Schematic diagram of experimental setup. (c) Dressed energy levels. (d) Splitting of fine structure energy level $|mj = \pm 1\rangle$.

$$\Gamma_{i/j} = \Gamma_{pop} + \Gamma_{ion-spin} + \Gamma_{ion-ion} + \Gamma_{phonon} - \Gamma_{dres\ \sin g} = \Gamma_{rad} + \Gamma_{non-rad} \quad (2)$$

Where Γ_{pop} is the population decay time, which depends on the location of the energy level in phase space. The terms ($\Gamma_{ion\text{-}spin}$+ $\Gamma_{ion\text{-}ion}$+Γ_{phonon}) are components of $(2\pi T^*_2)^{-1}$ (T^*_2 is the reversible transverse relaxation). The last term Γ_{rad} is the non-radiation decay time, which is related to the surface state of the Nano-/microcrystals. $\Gamma_{ion\text{-}spin}$ is related to the ion-spin coupling effect of the individual ion. $\Gamma_{ion\text{-}ion}$ is determined by the interaction among the ions of the crystal and can be controlled by the power of external field or impurity concentrations. Γ_{phonon} is related to the temperature of sample placed in a cryostat. Whereas, $\Gamma_{dressing}$ comes from dressed energy levels, the temporal intensity of the measured second-order FL from the density matrix element can be described as

$$I_{FL}(t) = I_0 e^{-G^2 t^2} \otimes \left|\rho^{(2)}_{11}\right| e^{-t\Gamma_{FL}(t)} \quad (3)$$

The two-mode intensity-noise correlation function $G^{(2)}_{ij}(\tau)$between intensity fluctuations of two optical beams as a function of time delay τ is given by

$$G^{(2)}_{ij}(\tau) = \frac{\langle \delta\hat{I}_i(t_i)\delta\hat{I}_j(t_j)\rangle}{\sqrt{\langle\left[\delta\hat{I}_i(t_i)\right]^2\rangle\langle\left[\delta\hat{I}_j(t_j)\right]^2\rangle}}\cos(\Delta\phi) \quad (4)$$

4. Results and DISCUSSIONS

Fig. 2 shows the time domain intensity signal of second-order FL obtained from different phases of Eu^{3+}:YPO_4 by fixing temperature at 77K. The intensity of the FL signal is related to density matrix elements. In Fig. 2, time-domain signals are obtained by fixing laser ***E*** at resonant wavelength. The resonant wavelength for T-phase YPO_4 and H-phase YPO_4 is measured at 592.3 nm and 589 nm, respectively. The measured resonant wavelength for two mixed-phase (T + H, H + T) YPO_4 is the same as T-phase YPO_4 i-e 592.3 nm. In Fig. 2, the decay rate measured for T-phase is almost four times (4 ms) as compared to the decay rate of H-phase (1 ms) as shown in Fig. 2(a). T-phase YPO_4 has D_{2d} site symmetry resonant peak results from population transfer from $|^7F_1, m_J = 0\rangle$ to $^5D_0$. Pure H-phase has D_2 site symmetry, and its resonant peak comes from particle transfer between $|^7F_1, m_{J=-1}\rangle$ to $^5D_0$. As both $|^7F_1, m_{J=0}\rangle$ and $|^7F_1, m_{J=-1}\rangle$ corresponds to different longitudinal relaxation time (T_1), reversible transverse relaxation rate T^*_2, hence, the different decay rate is observed for T-phase and H-phase YPO_4. However, the decay rate is observed maximum (11 ms) for mixed-phase (less H and more T) Eu^{3+}:YPO_4 shown in Fig. 2(c). This long decay rate can be explained from contribution from both T- and H-phases.

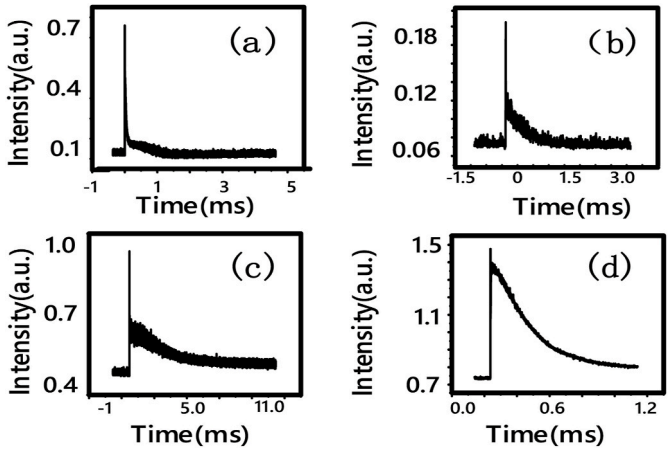

Fig. 2. Measured time-domain signal of second-order FL from (a) pure T-phase Eu^{3+}:YPO_4, (b) (less T-phase and more H-phase) Eu^{3+}:YPO_4, (c) (less H-phase and more T-phase) Eu^{3+}:YPO_4 and (d) pure H-phase Eu^{3+}:YPO_4.

In Fig. (3-5) and Fig. 7, we discussed spectral intensity in different phases of Eu3+: YPO4 (***E*** scanned from 585 nm to 599 nm) and Pr^{3+}:YPO_4 (***E*** scanned from 590 nm to 620 nm), respectively. The time domain signal contains both FL and spontaneous parametric four-wave mixing (SP-FWM) emission which can be distinguished by placing gate position at 10 μs and 15 μs, respectively. The excitation spectrum of different phases of Pr^{3+}:YPO_4 at different points of time-intensity signal is also discussed in detail in Fig. 7. A comparison of dressing effect in Eu^{3+}:YPO_4 and Pr^{3+}:YPO_4 has been presented. At last, we discussed evolution of two-mode intensity-noise correlation function by changing gate position for Pr^{3+}:YPO_4.

Fig. 3(a)–(d) shows the excitation spectrum of the FL signal measured from pure T-phase Eu^{3+}:YPO_4 crystal at different temperature. Fig. 3(a) shows the spectral intensity of FL obtained at room temperature (300K), where a first emission peak is observed at 592.3 nm followed by the second peak at 595.7 nm. The spectral distance between both peaks is 3.4 nm. Under the action of the crystal field of YPO_4, the term $^7F_1$ in magnetic dipole allowed transition ($^5D_0 \rightarrow {}^7F_J$) can split into a maximum of three fine structure levels (2J+1), as shown in Fig. 1(a). Theoretically, the maximum three emission peaks can be observed in T-phase Eu^{3+}:YPO_4 from three fine-structure energy levels. The Eu^{3+} ion is substituted for the Y^{3+} ions in pure T-phase YPO_4 contains D_{2d} site symmetry. In our experiment performed at 300 K, we observed only two peaks in T-phase YPO_4 (Fig. 3(a)), which suggests the site symmetry of D_{2d} is not strong enough to lift the 2J+1 degeneracy of the levels. The previous report suggests the crystal field split components and selection rule of the energy levels of the ground state $^7F_1$ in YVO_4 with the same D_{2d} symmetry [5]. However, a significant difference in splitting energy levels of $^7F_1$ is found between our work and the reported, our two emission peaks show a 3.4 nm interval as compared to that of 1.5 nm in published Eu^{3+}:YVO_4 sample [5]. This suggests that the split number of the $^5D_0 \rightarrow {}^7F_1$ transition is the same in the same site symmetry, but the split energy levels strictly depend on crystal composition or coordination environment. When the temperature is reduced to 200 K, other secondary peaks centered at 594.7 nm and 596.4 nm appear around the second peak, while the first peak remains unchanged (Fig. 3(b)) and those secondary peaks are obvious with further decrease in temperature (Fig. 3(c)). One can say that under the action of stress, degeneracy of energy level $|^7F_1, m_{J=\pm1}\rangle$ lifts and its splits into two levels i-e $|^7F_1, m_{J=1}\rangle$ and $|^7F_1, m_{J=-1}\rangle$. The two secondary peaks located at 595.7 nm and 596.4 nm come from energy levels $|^7F_1, m_{J=+1}\rangle$ and $|^7F_1, m_{J=-1}\rangle$, respectively. When the temperature is reduced to 77K, $\Gamma_{dressing}$ increases and phonon effect Γ_{phonon} becomes almost negligible, which reduces the total decay rate $\Gamma_{i/j}$ as suggested by equation (2). With a decrease in $\Gamma_{i/j}$ at 77 K, the linewidth of spectral signal reduces and the last three peaks become more obvious. This splitting of a single peak into three peaks results from the contribution of both stress and dressing effect. In tetragonal-phase Eu^{3+}:YPO_4, the splitting between two states $|^7F_1, m_{J=+1}\rangle$ and $|^7F_1, m_{J=-1}\rangle$ due to stress effect is measured close to 20 GHz, whereas the Rabi frequency is calculated at 1 GHz. Alone, Rabi frequency is not strong enough to split energy levels into multiple dressed states. Also, the self-dressing field E splits the state $|^7F_1, m_{J=-1}\rangle$ into two primary dressed states $|G\pm\rangle$ as shown in Fig. 3(f). If we set $|^7F_1, m_{J=-1}\rangle$ as the frequency reference point, the Hamiltonian can be written as $H = -h\begin{bmatrix} 0 & G_i \\ G_i^* & (-1)^i\Delta_i \end{bmatrix}$ from the equation$H|G_\pm\rangle = \lambda_\pm|G_\pm\rangle$, We can obtain $\lambda_+ = [(-1)^i\Delta_i + (\Delta_i^2 + 4|G_i|^2)^{1/2}]/2$and $\lambda_- = [(-1)^i\Delta_i - (\Delta_i^2 + 4|G_i|^2)^{1/2}]/2$. So the dressing field ***G*** makes the peak at 595.7 nm ($|^7F_1, m_{J=-1}\rangle$) as two dressed peaks. The YPO_4 has ground triplet state $^7F_1$ and singlet excited state $^5D_0$ (Fig. 1(a)). In Fig. 3(a), two spectral peaks located at 592.3 nm and 595.7 nm are from population transfer from sub-states, $|^7F_1, m_{J=1}\rangle$ and $|^7F_1, m_{J=0}\rangle$ to $^5D_0$, respectively. Fig. 3(f) shows the dressed energy levels caused by stress and dressing field

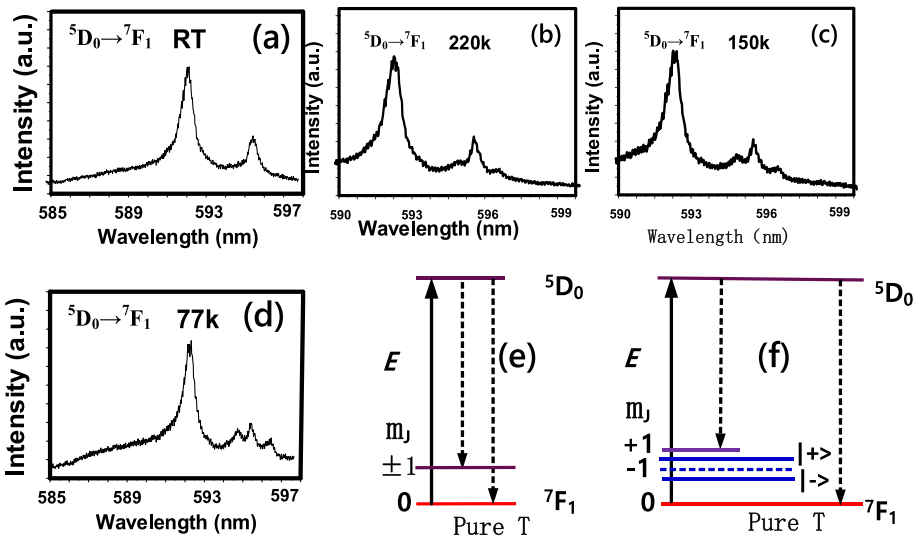

Fig. 3. Measured spectral intensity of FL signal obtained from T-phase Eu^{3+}:YPO_4 at (a) 300 K, (b) 220 K, (c) 150 K and (d) 77 K. (e) Fine structure energy levels of T-phase Eu^{3+}:YPO_4 (f) dressed energy levels of T-phase Eu^{3+}:YPO_4.

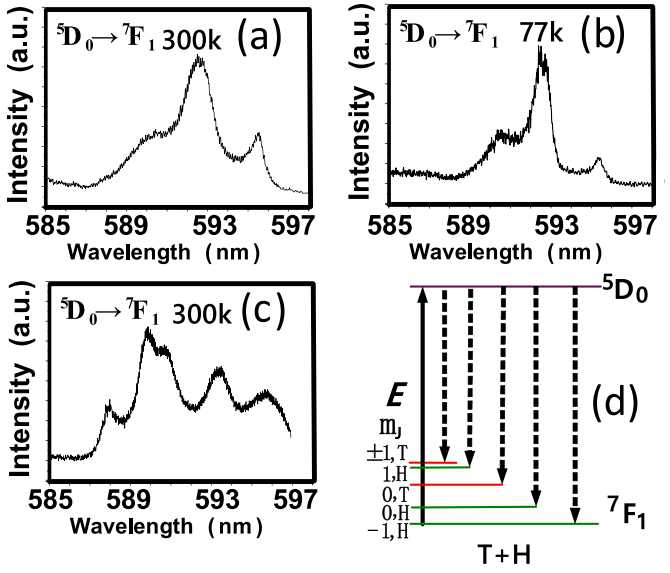

Fig. 4. The measured spectral intensity of FL signal obtained from (much T-phase and less H-phase) v at (a) 300K, (b) 77k. (c) Shows the spectral intensity of the FL signal obtained from (much H-phase and less T-phase) Eu^{3+}:YPO_4 at 300 K. (d) The fine structure splitting corresponding.to (c).

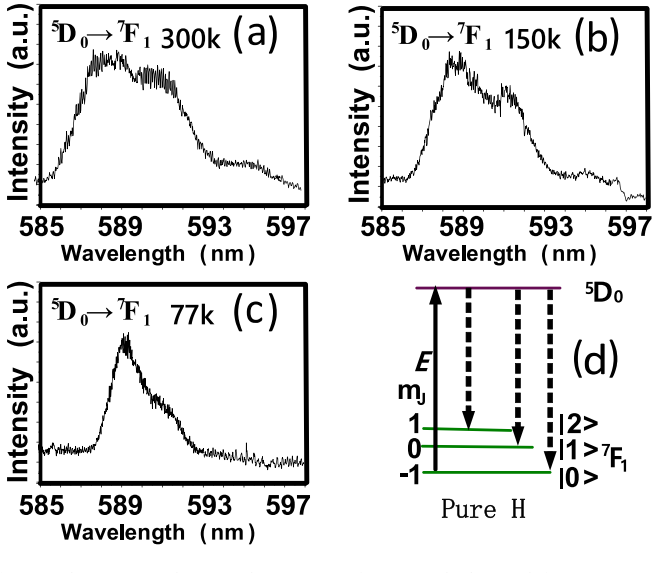

Fig. 5. The measured spectral intensity of FL signal obtained from pure H-phase Eu^{3+}:YPO_4 at (a) room temperature (b) 150K and (c) 77K. (d) The fine structure splitting in pure H-phase Eu^{3+}:YPO_4.

corresponding to three small peaks in Fig. 3(d).

Fig. 4(a) and (b) show the luminescence spectra of (much T-phase and less H-phase) Eu^{3+}:YPO_4 at 300 K and 77K, respectively. In Fig. 4(a), the excitation spectrum shows two sharp peaks centered at 592.3 nm and 595.7 nm with unresolved broadband on the left side of the first peak. As spectral positions of these two peaks are the same as peaks observed from T-phase (Fig. 3(a)), we can say that these two peaks come from T-phase. Then, the broadband should be attributed to Eu^{3+} emission from the H-phase of Eu^{3+}:YPO_4. The relatively low intensity of this band, compared with the higher intensity of the first sharp peak, is due to a little proportion (<10%) of the hexagonal phase in this mixed-phase as calculated from XRD [22]. In Fig. 4(b), when the temperature is changed to 77 K, the location of all three spectral peaks is the same as observed at 300K (Fig. 4(a)). At 77 K, the linewidth of the spectral signal is reduced, which can be explained from decrease in phonon Γ_{phonon} from Eq. (2).

Fig. 4(c) shows the measured luminescence spectrum taken from the different mixed phases, with 55% and 45% proportion of hexagonal and tetragonal phases, respectively. The luminescence spectrum (Fig. 4(c)) shows the highest one set of closely spaced but not well-resolved features centered at about 589 nm, and three well-resolved peaks are centered at 586.3 nm, 592.5 nm, and 595.7 nm. Spectral peaks measured at 592.5 nm and 595.7 nm corresponds to pure T-phase Eu^{3+}:YPO_4, as they are observed at the same positions of peaks observed from pure T-phase Eu^{3+}:YPO_4. In a mixed-phase (much H-phase and less T-phase) Eu^{3+}:YPO_4, the triplet state $^7F_1$ split into five fine levels (Fig. 4(d)), which corresponds to the five peaks illustrated in Fig. 4(c). The $|T, m_{J=1}>$ and $|T, m_{J=0}>$ belong to T-phase Eu^{3+}:YPO_4, the $|H, m_{J=1}>$, $|H, m_{J=0}>$ and $|H, m_{J=-1}>$ belong to H-phase Eu^{3+}:YPO_4.

Fig. 5 shows the luminescence spectrum of pure H-phase Eu^{3+}:YPO_4 at different temperatures. The Eu^{3+} ions in H-phase Eu^{3+}:YPO_4 occupy D_2 site symmetry, which is a subgroup of D_{2d}. For doping ions, this symmetry can completely lift the 2J+1 degeneracy of the ^7F_J levels suggested by the allowed transition lines at 32 crystallographic point

groups. Theoretically, three peaks should be observed for $^5D_0 \rightarrow {}^7F_1$ transition in the hexagonal phase of Eu^{3+}:YPO_4. However, there is no defined calculation and experimental evidence that how the peak located at 586.3 nm and the unresolved set at 589 nm is observed in mixed-phase., To understand this, it is necessary to measure pure hexagonal phase. In Fig. 5(c), the effect of phonon Γ_{phonon} is decreased at low temperatures, which leads to a reduced Γ_{ij} rate. As Γ_{FL} is reduced, the linewidth of FL spectral will be reduced because of the increased $\rho_{11}^{(2)}$ in equation (1). The linewidth of the spectral peak is narrow as compared to peaks observed in Fig. 5(a) and (b). In Fig. 5(d), three split fine structure levels $|^7F_1, m_{J=1}\rangle$, $|^7F_1, m_{J=0}\rangle$ and $|^7F_1, m_{J=-1}\rangle$ corresponds to three peaks observed in Fig. 5(b).

Table 1 presents the observed peak positions in each phase. Comparing the spectrum of a pure H- and T-phase Eu^{3+}:YPO_4 the spectrum of the mixed-phase in Fig. 4 can be regarded as the superposition of spectrums of two pure phases. Furthermore, four phases have different space groups, whereas the tetragonal phase is more asymmetric than the hexagonal phase, which due to its more atomic-like system. .[4]

Since Pr^{3+}:Y_2SiO_5 crystal and Eu^{3+}:YPO_4 crystals are atom-like systems and similar to Pr^{3+}:Y_2SiO_5 crystal's [23] Since both Pr^{3+}:YPO_4 and Eu^{3+}:YPO_4 crystals are atom-like systems which possesses similar properties as Pr^{3+}:Y_2SiO_5 crystal. [23] The Eu^{3+}:YPO_4 crystal used in our experiment has powder form, whose defects on crystal surface influences the polarization of the incident field, making it difficult to predict in terms of mathematics and physics. [23,24] So in Fig. 6, we predict the hyperfine Zeeman energy-levels of three different phases of Eu^{3+}:YPO_4 i-e (pure T-phase, pure H-phase, (less T and more H)-phase), which are quite similar to that of Pr^{3+}:Y_2SiO_5 crystal's.

In Fig. 6, we briefly predict the hyperfine Zeeman energy-levels of three phases (pure T-phase Eu^{3+}:YPO_4, pure H-phase Eu^{3+}:YPO_4, (less T, and more H)-phase Eu^{3+}:YPO_4) with Clebsch-Gordan (CG) coefficients by demonstrating transition paths among Zeeman sublevels when exciting field's polarization is switched from linear to circular. When $\boldsymbol{E}$ is linearly polarized, only to or to ($m_J = -1, 0, 1$; $m_I = 1/2, \pm 3/2, \pm 5/2$) vertical transition pathways are allowed. When the polarization is changed to right-circular and left-circular, these polarized beams drive the transitions from $|m_J, m_I\rangle$ to $|m_J, m_{I+1}\rangle$ or from $|m_J, m_I\rangle$ to $|m_J, m_{I-1}\rangle$.

Fig. 7 shows the spectral intensity signal of Pr^{3+}:YPO_4 when the power of $\boldsymbol{E}$ is increased from low (1 mW) to high (9 mW). To measure the spectral signal, input field $\boldsymbol{E}$ is scanned from 590 to 620 nm by fixing gate position (1 μs) and temperature (77 K). The powers of $\boldsymbol{E}$ are changed from low to high, the spectral signal switches from enhancement peak (Fig. 7(a1)) to dressing suppression dip (Fig. 7(a5)). Initially, the spectrum signal with a Lorentzian line shape enhancement peak is observed at a lower power level, as shown in Fig. 7(a1). When power is increased, the FL signal evolves from Autler–Townes-like splitting to pure suppression, caused by the dressing effects of $\boldsymbol{E}$ $|G|^2/(\Gamma_{10} + i\Delta)$ (from Eq. (1)), as shown in Fig. 7(a4)–7(a5). Especially, the FL signal is completely suppressed at the maximum $\boldsymbol{E}$ power (9 mW), which can be described by the dressed energy levels shown in Fig. 1(c). Fig. 7(b) shows the excitation spectrum for much H-phase and less T-phase Pr^{3+}:YPO_4. In Fig. 7(b1)), no enhancement peak is obsserved at low power, which can be explained from strong dressing effect in much H-phase and less T-phase Pr^{3+}:YPO_4. As $\boldsymbol{E}$ power increases, dressing effect $|G|^2/(\Gamma_{10} + i\Delta)$ increases resulting in strong dressing suppression dip observed in Fig. 7(b5). Fig. 7(c) shows spectral intensity signal for pure T-phase Pr^{3+}:YPO_4, which follows similar behavior concerning an increase in power as explained from Fig. 7(a). By comparing Fig. 7(a–c), we can conclude that switch between enhancement peak to dressing suppression dip can only be observed for a phase having low sensitivity of dressing effects such as pure T-phase Pr3+:YPO_4.

Table 1
The peak location of $^5D_0$ to $^7F_1$ and the cross bonding energy of peak location of four different phases of Eu^{3+}:YPO_4.

Phase	The peak locations of $^5D_0$ to $^7F_1$ (nm)				The corresponding ground states (<|m_J>)			
Pure H	586.3	589.0		595.7	|−1>	|0>		|1>
PureT			592.3	595.7			|0>	|±1>
More H + Less T	586.3	589.0	592.5	595.7	|−1>H	|0>, H	|0>, T	|1>,H |±1>, T
Less H + More T		589.0	592.3	595.7		|0>, H	|0>, T	|1>,H |±1>, T

By comparing dressing effect of Eu^{3+}:YPO_4 (Fig. 3(d)) with Pr^{3+}:YPO_4 (Fig. 7(c4))) by fixing laser power (7 mW) and temperature (77K), we observed that the dressing effect is much stronger in Pr^{3+}:YPO_4 as shown in Fig. 7(c4). This can be explained from higher dipole moment of Pr_{3+}:YPO_4 as compare to Eu_{3+}:YPO_4 which corresponds to stronger dressing effect.

Herein, we investigated the two-mode intensity noise correlation of anti-Stokes and composite (FL + $\boldsymbol{E_S}$) signals by changing position form 200 ns to 5 μs. The time-dependent intensity fluctuations of the $\boldsymbol{E_{AS}}$ signal from PMT2 and composite signal from PMT1 are plotted as a function of delayed time using Eq. (4). The total intensity of the composite signal is given by $\rho_{11}^{(2)} + \rho_S^{(3)}$. The input beam $\boldsymbol{E}$ is excited on sample at resonant wavelength ($\Delta = 0$) at medium power (5 mW) when temperature of cryostat is fixed at 77K. When input field E is open, third-order Stokes is generated along with SP-FWM process, considering the dressing terms and the perturbation chain.

$\rho_{00}^{(0)} \xrightarrow{E_1} \rho_{10}^{(1)} \xrightarrow{E_{AS}} \rho_{11}^{(2)} \xrightarrow{E_1'} \rho_{10(S)}^{(3)}$ the third-order nonlinear density matrix elements for Stokes can be written as $\rho_{10(S)}^{(3)} = -iG_{AS}G_1G_1'/[(\Gamma_{10} + i\Delta_1)(\Gamma_{00} - i\Delta_1' + |G_1|^2/\Gamma_{00} - i\Delta_1)\Gamma_{11}]$.

Fig. 8(a) shows the two-mode intensity-noise correlation $G^{(2)}(\tau)$ obtained from (much T and less H)-phase Eu^{3+}:YPO_4 at different gate position. When gate position is changed from 200 ns to 5 μs, hybrid lineshape of correlation function changes from sharp (Fig. 8(a1)) to broad (Fig. 8(a4)) which can be explained from evolution of $\boldsymbol{E_S}$ from pure FL in composite signal [24,25]. When gate positon is at 200ns, FL emission dominates over $\boldsymbol{E_S}$ in composite signal due to low lifetime of FL corresponding to sharp lineshape of correlation as observed in Fig. 8(a1) [26]. As gate position increases, the proportion of $\boldsymbol{E_S}$ in composite signal increases significantly. Spectral linewidth of $\boldsymbol{E_S}$ is determined by the atomic coherence time and are thus much narrower corresponding to broad peak correlation throughout Fig. 8(a4). The evolution of linewidth of correlation function broad to sharp can be explained from change in initial phase as FL is transferred to $\boldsymbol{E_S}$. In Eu^{3+}:YPO_4, dressing effect is not strong enough to induce non-linear phase strong enough to cause switch in correlation. Fig. 8(b) shows two-mode correlation obtained from (much T and less H)-phase Pr^{3+}:YPO_4. Unlike Eu^{3+}:YPO_4, correlation measured for Pr^{3+}:YPO_4 shows switches from negative (Fig. 8(b1)) to positive (Fig. 8(b4)) as gate position is changed from 200 ns to 5 μs. The switching of correlation peak from negative to positive can be explained by cross phase modulation (XPM) and self phase modulation (SPM) induced in the composite channel due to the nonlinear Kerr effect, The SPM and XPM generate the nonlinear ($\Delta\phi_N$) and initial phase ($\Delta\phi_I$) in the composite channel, respectively, which can be mathematically modeled as $\Delta\phi = \Delta\phi_N + \Delta\phi_I$. Where $\Delta\phi_N = \phi_S - \phi_{AS} = 2(n_2^s|E_S|^2 + n_2^x|E_{AS}|^2)\varsigma e^{-r^2} z/n_1^{S/AS}$ and $\Delta\phi_I = \phi_S - \phi_{FL} = 2(n_2^s|E_S|^2 + n_2^{FL}|E_{FL}|^2)\varsigma e^{-r^2} z/n_1$. As discussed above, the FL dominates when gate position is at 200ns. Due to strong contribution of nonlinear phase and initial phase, total phase difference between composite signal FL and $\boldsymbol{E_{AS}}$ approaches $\Delta\phi = \pi$, which results in negative-correlation observed in Fig. 8(b1). As gate position increases, $\boldsymbol{E_S}$ proportion in composite signal increases significantly. When gate position is increased to 5 μs, the composite signal behaves like pure $\boldsymbol{E_S}$ signal and correlation curve is switched from negative to positive (Fig. 8

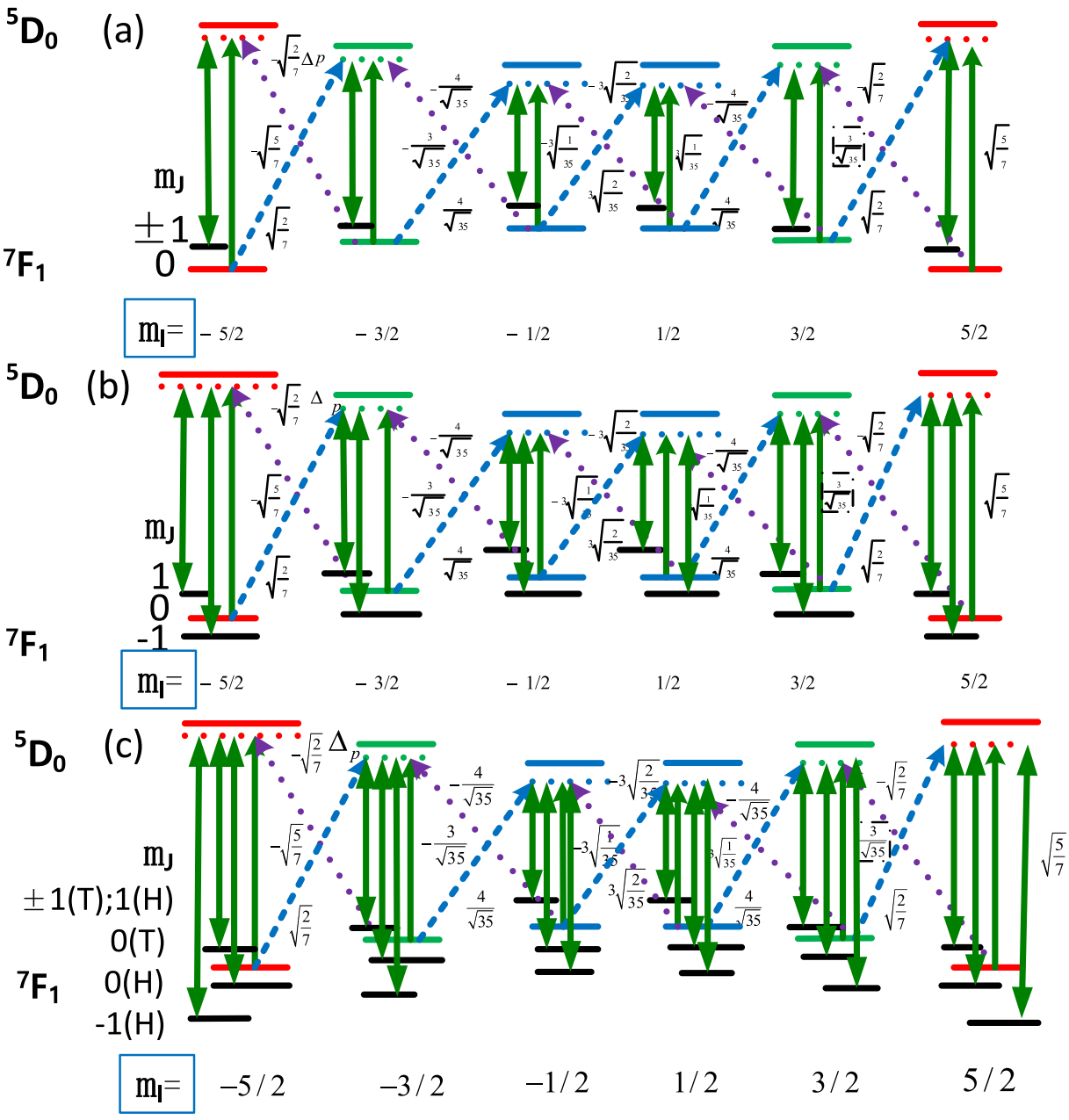

Fig. 6. Zeeman energy levels and transition paths at different polarization states (linear, left circular and right circular polarization) with three different phase. (a) The Zeeman energy level of pure T-phase Eu^{3+}:YPO_4, (b) Pure H-phase Eu^{3+}:YPO_4, and (c) (less T and more H)-phase Eu^{3+}:YPO_4.

(b4)). As gate position increases, effect of nonlinear phase and initial phase reduces and total phase for $G^{(2)}(\tau)$changes from$\Delta\phi \approx \pi$ to $\Delta\phi \approx 0$ which causes a switch in correlation curve observed in Fig. 8(b4).

By comparing effect of different doped ion, we can conclude correlation switches from negative to positive in Pr^{3+} ion whereas one linewidth of correlation is changed from broad to sharp in Eu^{3+} ion. As discussed in Fig. 7, dressing effect in stronger in Pr^{3+}:YPO_4 as compare to Eu^{3+}:YPO_4 due to higher dipole moment. Due to stronger dressing effect, nonlinear phase induced in Pr^{3+}:YPO_4 is strong causing switch in correlation curve as shown in Fig. 8(b). In case of in Eu^{3+}:YPO_4, nonlinear phase induced is not strong enough to cause switch in two-mode correlation. From Fig. 8(a)-8(b), we can also conclude that linewidth of correlation function can be controlled through initial phase where correlation switch can be obtained through strong nonlinear phase.

5. Conclusion

In summary, the crystal field splitting of fine spectra in Eu^{3+}:YPO_4 and Pr^{3+}:YPO_4. crystal with different phase transitions are investigated. For pure T-phase Eu^{3+}:YPO_4, triple splitting of fine structures with 595.7 nm and 592.3 nm can be observed at 77K. Fine structure splitting can be observed for pure H-phase Eu^{3+}:YPO_4 with spectral peaks observed at 586.3 nm, 589.0 nm and 595.7 nm. The splitting of fine structure can also be observed at low temperatures but only for the (more T and less H)-phase Eu^{3+}:YPO_4, the splitting of fine structures is at about 596.3 nm, 589 nm, 592.5 nm and 595.7 nm respectively. The line width of crystal field splitting of fine are observed to be narrow due to reduced phonon effect caused by low temperature. As for Pr^{3+}:YPO_4 the, switching only happened in pure H-phase Pr^{3+}:YPO_4 and mixed phase (much H and less T) Pr^{3+}:YPO_4. We predict the Zeeman energy level from pure T-phase Eu^{3+}:YPO_4, pure H-phase Eu^{3+}:YPO_4, and mixed

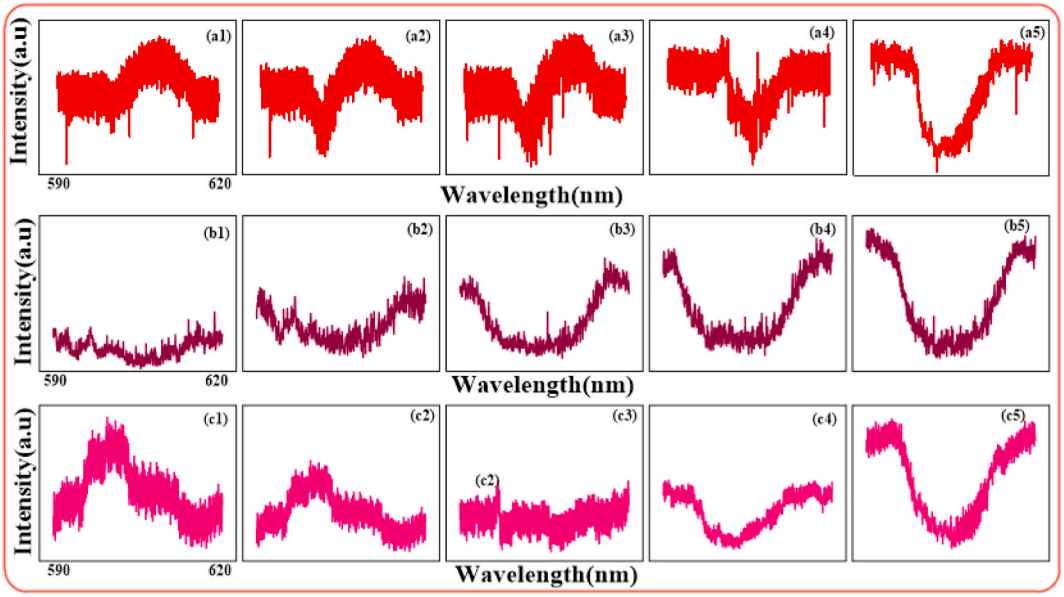

Fig. 7. Measured spectral-domain signal by changing the power of ***E*** from 1 mW to 9 mW while temperature and gate position are fixed at 77 K and 1 μs, respectively, from (a) much T-phase and less H-phase Pr^{3+}:YPO_4, (b) (much H-phase and less T-phase) Pr^{3+}:YPO_4 and (c) Pure T-phase Pr^{3+}:YPO_4.

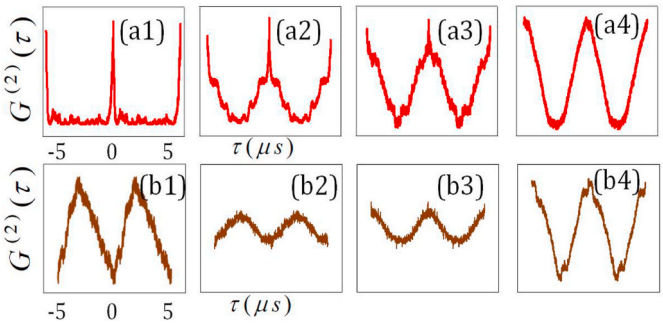

Fig. 8. Two-mode intensity-noise correlation between composite signal (FL + E_S) and E_{AS} versus delayed time τ obtained by changing gate position from 200 ns to 5 μs (a) (much T and less H)–phase Eu^{3+}:YPO_4 (b) (much T and less H)–phase Pr^{3+}:YPO_4.

phases. We predicted that the strong atomic-like behavior of H-phase Pr^{3+}:YPO_4 should have strong dressing effect. Furthermore, by investigating effect of different doped ion on two-mode intensity-noise correlation we found out that correlation switch is observed in Pr^{3+}:YPO_4 due to strong dressing effect resulting from higher dipole moment as compare to Eu^{3+}:YPO_4. Also, we observed that nonlinear phase can cause switch from anti-correlation whereas initial phase can be used to control linewidth of correlation from sharp to broad.

Declaration of competing interest

The authors declare that they have no known competing financial interests or personal relationships that could have appeared to influence the work reported in this paper.

Acknowledgment

This work was supported by the National Key R&D Program of China (2017YFA0303700, 2018YFA0307500), National Natural Science Foundation of China (61975159, 61605154, 11604256, 11804267, 11904279).

Appendix A. Supplementary data

Supplementary data to this article can be found online at https://doi.org/10.1016/j.jlumin.2020.117702.

References

[1] C.G. Ma, A.V. Popov, A.S. Vanetsev, O.M. Gaitko, E.O. Orlovskaya, S. Lange, I. Sildos, V. Orlovskii Yu, "Vacuum ultraviolet spectroscopic analysis of Ce3+-doped hexagonal YPO4• 0.8H2O based on exchange charge model, J. Lumin. 152 (2014) 70–74.
[2] A.S. Vanetsev, E.V. Samsonova, O.M. Gaitko, K. Keevend, A.V. Popov, U. Mäeorg, H. Mändar, I. Sildos, V. Orlovskii Yu, Phase composition and morphology of nanoparticles of yttrium ortanti_hophosphates synthesized by microwave-hydrothermal treatment: the influence of synthetic conditions, J. Alloys Compd. 639 (2015) 415–421.
[3] A. Arakcheeva, D. Logvinovich, G. Chapuis, V. Morozov, S.V. Eliseeva, J.C. G. Bunzli, P. Pattison, ", The luminescence of NaxEu3+(2−x)/3MoO4 scheelites depends on the number of Euclusters occurring in their incommensurately modulated structure, Chem. Sci. 3 (2012) 384–390.
[4] P. Li, Y.P. Zhang, L. Zhang, Guo Y.X. Li, Y.H. Li, W.P. Gao, Phase control of Eu3+ doped YPO4 nano-/microcrystals, Cryst. Growth Des. 11 (2017) 5935–5944.
[5] M.N. Luwang, R.S. Ningthoujam, Jagannath, S.K. Srivastava, R.K. Vatsa, ", Effects of Ce3+ codoping and annealing on phase transformation and luminescence of Eu3+-doped YPO4 nanorods: D2O solvent effect, J. Am. Chem. Soc. 132 (2010) 2759–2768.
[6] M.N. Luwang, R.S. Ningthoujam, S.K. Srivastava, R.K. Vatsa, Disappearance and recovery of luminescence in Bi3+, Eu3+ codoped YPO4 nanoparticles due to the presence of water molecules up to 800°C, J. Am. Chem. Soc. 133 (2011) 2998–3004.
[7] J.C.G. Bunzli, S.V. Eliseeva, Intriguing aspects of lanthanide luminescence, Chem. Sci. 4 (2013) 1939–1949.
[8] Christiane Görller-Walrand, Koen Binnemans, Rationalization of crystal-field parametrization Handbook on the physics and chemistry of rare earths 23 (1996) 121–283.
[9] G.R. Choppin, J.C.G. Bünzli, Lanthanide probes in life, chemical and earth sciences [J], CG Bunzli GR Choppin Elsevier Amsterdam (1989) 219.
[10] B.R. Judd, Optical absorption intensities of rare-earth ions[J], Phys. Rev. 127 (1962) 750.
[11] G.S. Ofelt, "Intensities of crystal spectra of rare-earth ions[J], J. Chem. Phys. 37 (1962) 511–520.
[12] X.Y. Chen, G.K. Liu, The standard and anomalous crystal-field spectra of Eu3+[J], J. Solid State Chem. 178 (2005) 419–428.
[13] X.Y. Chen, W. Zhao, R.E. Cook, G.K. Liu, ", Anomalous luminescence dynamics of Eu 3+ in BaFCl microcrystals[J], Phys. Rev. B 70 (2004) 205122.
[14] H. Zheng, X. Zhang, Z. Zhang, Y. Tian, H. Chen, C. Li, Y. Zhang, Parametric amplification and cascaded-nonlinearity processes in common atomic system, Sci. Rep. (2013) 31885.
[15] A. Lipsich, S. Barreiro, A.M. Akulshin, A. Lezama, Absorption spectra of driven degenerate two-level atomic systems, Phys. Rev. 61 (2000), 053803.

[16] V. Milner, Y. Prior, Multilevel dark states: coherent population trapping with elliptically polarized incoherent light, Phys. Rev. Lett. 80 (1998) 940–943.
[17] Y. Du, Y. Zhang, C. Zuo, C. Li, Z. Nie, H. Zheng, M. Xiao, Controlling four-wave mixing and six-wave mixing in a multi-Zeeman-sublevel atomic system with electromagnetically induced transparency, Phys. Rev. 79 (2009), 063839.
[18] M.C. Phillips, H. Wang, I. Rumyantsev, N.H. Kwong, R. Takayama, R. Binder, Observation of ultraslow and stored light pulses in a solid, Phys. Rev. Lett. 88 (2002), 023602.
[19] S.H. Autler, C.H. Townes, Stark effect in rapidly varying fields, Phys. Rev. 100 (1955) 703.
[20] B. Walker, M. Kaluza, B. Sheehy, P. Agostini, L.F. DiMauro, Observation of continuum-continuum Autler-Townes splitting, Phys. Rev. Lett. 75 (1995) 633.
[21] Y. Zhang, A.W. Brown, M. Xiao, Opening four-wave mixing and six-wave mixing channels via dual electromag netically induced transparency windows, Phys. Rev. Lett. 99 (2007) 123603.
[22] P. Li, Y. Liu, Y.X. Guo, X.L. Shi, G.Q. Zhu, H. Zuo, Hydrothermal synthesis of YPO4: Eu3+ hexagonal prisms microarchitectures: tunable morphology, formation mechanism, and recovery luminescence properties, Ceram. Int. 41 (2015) 6620–6630.
[23] K. Gawlitza, S.T. Turner, F. Polzer, et al., Interaction of gold nanoparticles with thermoresponsive microgels: influence of the cross-linker density on optical properties, [J]," Phys. Chem. Chem. Phys. 15 (37) (2014) 15623–15631.
[24] Y. Xu, X. Ma, J. Hu, et al., Structures and energetics of low-index stoichiometric BiPO4 surfaces[J], Phys. Cryst. Eng. Comm. 21 (2019).
[25] Faizan Raza, et al., Hybrid switch of correlation and squeezing using resonant and off-resonant excitation spectrum in Nitrogen-vacancy center diamond, IEEE Photonics Journal 11 (5) (2019) 1–10.
[26] H. Fan, A. Imran, F. Raza, K. Amjad, P. Li, Y. Zhang, Double cascade dressed MOSFET from doped Eu^{3+} and Pr^{3+} in a host YPO_4, RSC Adv. 9 (2019) 38828.